Transport properties of Na doped $La_{1-x}Ca_{x-y}Na_yMnO_3$ measured in a pulsed magnetic field

2002 J. Phys.: Condens. Matter 14 10221

(http://iopscience.iop.org/0953-8984/14/43/319)

INSTITUTE OF PHYSICS PUBLISHING JOURNAL OF PHYSICS: CONDENSED MATTER

J. Phys.: Condens. Matter **14** (2002) 10221–10235 PII: S0953-8984(02)36776-6

Transport properties of Na doped $La_{1-x}Ca_{x-y}Na_yMnO_3$ measured in a pulsed magnetic field

Sayani Bhattacharya[1], Aritra Banerjee[1], S Pal[1], P Chatterjee[2], R K Mukherjee[1] and B K Chaudhuri[1,3,4]

[1] Department of Solid State Physics, Indian Association for the Cultivation of Science, Jadavpur, Kolkata-700 032, India
[2] Department of Physics, Vivekananda Mahavidyalaya, Hariipal, Hooghly-712405, India
[3] Department of Physics, National Sun Yat Sen University, Kaohsiung-804, Taiwan, Republic of China

E-mail: sspbkc@rediffmail.com (B K Chaudhuri)

Received 2 May 2002, in final form 6 August 2002
Published 18 October 2002
Online at stacks.iop.org/JPhysCM/14/10221

Abstract

Temperature-dependent magnetization and magnetoresistance of the Na doped $La_{1-x}Ca_{x-y}Na_yMnO_3$ type samples with $x = 0.3$ and $0 \leqslant y \leqslant 0.15$, showing a rhombohedrally distorted perovskite structure with space group $R\bar{3}c$, have been studied under a pulsed magnetic field. With the increase in temperature from the low temperature ferromagnetic phase, the samples exhibit a sharp metal to insulator transition around T_p accompanied by a ferromagnetic (metallic) to paramagnetic (semiconducting) phase transition with a well defined Curie temperature T_C (almost equal to T_p). Interestingly, small Na doping largely increases the conductivity and T_p, which is associated with a decrease of the (e–ph) interaction constant (γ). Doping of monovalent Na in the Ca site of $La_{1-x}Ca_{x-y}Na_yMnO_3$ drives the system from a high resistivity regime with lower T_p to a lower resistivity regime with higher T_p values. Low temperature resistivity data fit well the relation $\rho = \rho_0 + \rho_2 T^2$, signifying the importance of the electron–magnon scattering process (the $\rho_2 T^2$ term). On the other hand, the high temperature ($T > T_p$ up to 320 K) conductivity data satisfy the variable range hopping (VRH) model. For $T > 320$ the small polaron hopping model is more appropriate than the VRH model. Even with a very small change of y, the density of states at the Fermi level $N(E_F)$ changes considerably. The resistivity of these materials measured under pulsed and continuous DC magnetic fields behaves in an identical fashion. The relaxation time (decay time of the magnetic pulse within the sample) varies with field strength, which indicates that, with a change of magnetic field, the ordering of spin in the ferromagnetic regime changes.

[4] Author to whom any correspondence should be addressed.

1. Introduction

Perovskite-like compounds obtained from the insulating $LaMnO_3$ by partial substitution of the divalent ion in La^{3+} have long been known [1]. But recently these materials have attracted considerable attention worldwide because of their remarkable large magnetoresistance (CMR) behaviour [2]. The study of their magnetotransport properties is of great significance both for understanding the basic mechanism of the metal–insulator transition (MIT) in these strongly correlated electron systems and also for their potential applications in devices, recorder heads, etc. It was believed that the spin structure and the electronic properties of $R_{1-x}A_xMnO_3$ (R = rare-earth metal, A = divalent element) were correlated via the double-exchange (DE) mechanism controlled by the motion of the e_g electrons from Mn^{3+} to Mn^{4+} sites [3]. However, Millis *et al* [4] argued that DE alone could not explain the CMR and other properties like the heat capacity anomaly around MIT in $R_{1-x}A_xMnO_3$ and it was proposed that a strong electron–phonon coupling, leading to Jahn–Teller effects, should also play an important role. Moreover, the average sizes of the R [5–7] and A [8, 9] site cations, the 'mismatch effect' [10], the vacancy in R and Mn sites [11] and the oxygen stoichiometry [12, 13] play a crucial role. Magnetic and electronic phase diagrams were established for $R_{1-x}A_xMnO_3$ to represent lattice effects. Archibald *et al* [14] suggested an unusual trapping out of mobile holes above T_C due to local static Jahn–Teller deformation. Until now, most of the studies on rare earth manganites concentrated on divalent ion doped $R_{1-x}A_xMnO_3$ compounds (A = Ca, Sr, Pb, Ba, etc) and most of them crystallize in an orthorhombically distorted perovskite structure (O'-type; $c/2 < a < b$; space group $Pbmn$) with a cooperative ordering of Jahn–Teller distorted $Mn^{3+}O_6$ octahedra [15]. In contrast, there are only a few reports of monovalent alkali-metal ion doped compounds [16–19]. Alkaline-earth metal and alkali doping on $LaMnO_3$ can lead to different consequences; the latter can lead to less inhomogeneity, because fewer impurity ions are needed to achieve a specific carrier concentration and larger random potential fluctuations being experienced by the electrons in the σ^* bond due to the larger difference in valence between La^{3+} and alkali-metal ions [20]. Since the valence state of the alkali-metal ions is +1, substitution with these ions affect the ratio of Mn^{3+} ($t_{2g}^3e_g^1$: S = 2) and Mn^{4+} ($t_{2g}^3e_g^0$: S = 3/2) ions which ultimately affects the DE mechanism.

Studies on the compounds (in La sites) like La–Na–Mn–O, La–K–Mn–O and La–Sr–Na–Mn–O [16–19] does not exhibit any consensus on the effect of Na doping on T_p and transport properties. All these prompted us to study the effect of monovalent alkali (Na) substitution in the Ca site. Apparently it seems that the effect of Na doping would have an identical effect to that of increasing the Ca content (up to 33%), but our observation shows a different result. The origin of the increase in T_p is not the same in both cases. It is also worth mentioning that, so far, conductivity, magnetoresistance and thermoelectric power of the CMR materials have been measured mostly under a continuous (DC) magnetic field. So we used a pulsed magnetic field to study the transport properties of the selected samples, giving identical results to those obtained under a DC magnetic field. Obviously, the advantage of the pulsed field technique is that one can use low and high fields of short duration, using a relatively easy process, for studying the magnetic properties of solid samples. Moreover, as the field is produced for a very short period, the heating effect is not very pronounced.

In this work we have prepared a novel manganite series $La_{1-x}Ca_xMnO_3$, where Ca^{2+} ions have been partially replaced by Na^+, K^+ and Li^+. The present paper deals with the effect of Na substitution, showing an increase in conductivity and T_p with increasing Na content. Experimental data have been analysed with existing theoretical models. Momentary excitation of the magnetic spins with a pulsed field and the corresponding time of their return to the normal state (relaxation time) has also been measured, indicating spin ordering in the sample.

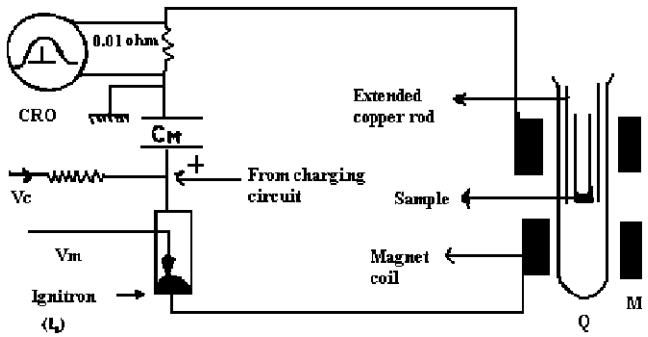

Figure 1. Circuit diagram for pulsed magnetic field generation. M: magnet coil, C_M: main capacitor, Q: quartz tube, CRO: digital storage oscilloscope.

2. Experimental details

2.1. Sample preparation

$La_{1-x}Ca_{x-y}Na_yMnO_3$ type samples (with $x = 0.3$ and $y = 0.0, 0.05, 0.1, 0.15$) were prepared by a standard ceramic processing technique. Well mixed stoichiometric mixtures of La_2O_3, CaO, Na_2CO_3 and $(CH_3COO)_2Mn$, $4H_2O$ (each of purity >99%) were first heated to 773 K and then to 1073 K for 5 h with intermediate grinding and then again annealing at 1173 K for 48 h. The sintered powder thus obtained was ground, pelletized and annealed again at 1073 K for 72 h and then furnace cooled. X-ray powder diffraction (XRD) studies have been carried out with Cu Kα radiation for structural studies. Chemical analysis indicates the presence of sodium ions in the samples.

2.2. Arrangement for resistivity measurement under pulsed magnetic field

For resistivity measurement, a standard constant current source (of magnitude 50.0 mA) was used and for the magnetoresistance study under a pulsed field, we used a lab-made set-up of a pulsed magnetic field produced in an air-core solenoid coil by sudden discharge of a capacitor bank (figure 1). The crystal was mounted on the tail-end part of the modified closed cycle helium cryostat (Displex, Air Products) made by attaching a copper rod onto the lower part of the original Displex. For good electrical contact gold electrodes (films) were first made on the sample surface by a vacuum sputtering technique and the electrical contacts of the leads and the sample were made with good-quality quickly drying silver paint. To avoid the induction effect (spurious) that arises due to the introduction of a metallic sample into the magnetic field, data were taken at the peak of the pulsed field where the induction effect is zero. The sample placed nearly at the centre of the solenoid coil feels a pulsed magnetic field in a vertical direction whenever a surge of current passes through the coil. The strength of the magnetic field is varied by varying the capacitor voltage with the help of a variac. In the present case, we have taken measurements with a maximum magnetic field of 4.4 T and between 300 and 15 K (or, for some samples, between 350 and 15 K). The peak value of the magnetic field is measured utilizing the following procedure.

The induced voltage in the usual pick-up coil is used to determine the magnetic field. It is seen that the shape of the current, which is proportional to the transient magnetic field inside the coil, is that of a single half period of a sine wave. This shape corresponds to a lumped LCR oscillation (figure 2(A)). The oscilloscope tracing of the nature of the current passing

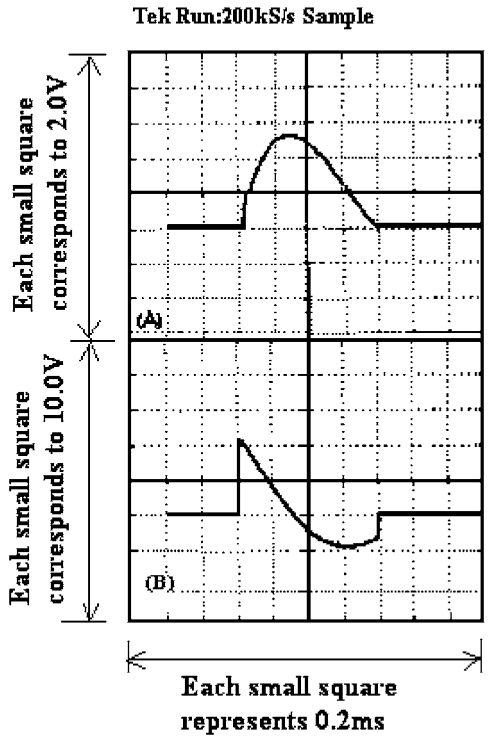

Figure 2. (A) The CRO trace of the current (measured across a 0.01 Ω resistance) discharging the capacitor bank at 2.5 kV which produces the pulsed magnetic field, and (B) the corresponding induced voltage in the 15-turn pick-up coil made of 1 mm thick wire.

through the coil and the corresponding induced voltage across a pick-up coil (of 15 turns and 1 mm diameter) are shown in figures 2(A) and (B), respectively. As observed from figure 2(A), the field starting from zero reaches a maximum and again returns to zero in about 572 μs for the coil used and the maximum value of the surge current through the magnet coil can be measured by finding the voltage across a standard resistance of 0.01 Ω connected in series with the magnet coil. The shape of the voltage in the pick-up coil placed inside the magnet coil corresponds to the derivative of the field inside the coil. The induced voltage in the pick-up coil placed in a time varying magnetic field B inside the air core main solenoid is given by, $V_i(t) = S(\mathrm{d}B/\mathrm{d}t)$ at any instant. $\mathrm{d}B/\mathrm{d}t$ is maximum at the start and end of the magnetic field and it is zero at the peak of the field. The voltages on either side of 0 V in the pick-up coil is of opposite sign as it should be, because on two sides of B_m, $\mathrm{d}B/\mathrm{d}t$ is of opposite sign and S is the effective area of the pick-up coil. When the coil has N number of turns, each of cross sectional area φ, and is placed with its axis parallel to the field lines, one can write $S = N\varphi + S_a$, where S_a is an active area formed by the leads and connections. S_a becomes negligible for a simple pick-up coil made of thin wire and here $S = N\varphi$. If we denote by t_m the time for which the pulsed magnetic field is at its peak (B_m), we have

$$B_m = \frac{\int_0^{t_m} V_i(t)\,\mathrm{d}t}{S}.$$

For each pick-up coil we have taken the $V_i(t)$ data repeatedly by the digital storage oscilloscope (Model Iwatsu, DS-6612, 60 MHz) and these data are averaged. In order to measure the peak field, the area of the positive triangle (upper) formed by $V_i(t)$ against t_m,

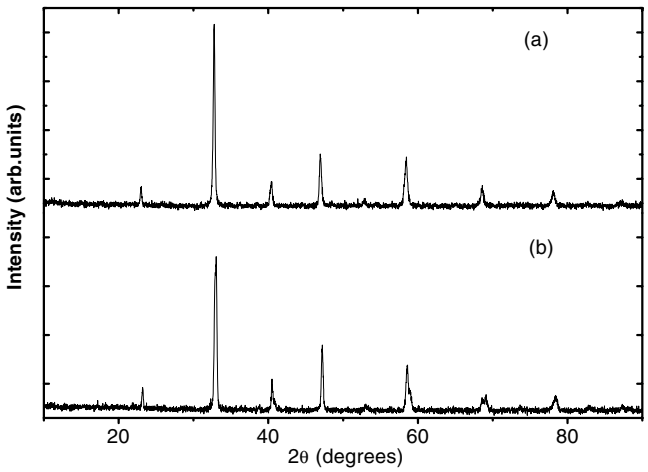

Figure 3. XRD pattern of the sample $La_{1-x}Ca_{x-y}Na_yMnO_3$ taken at room temperature with Cu Kα radiation (a) with $x = 0.3$ and $y = 0.0$, (b) with $x = 0.3$ and $y = 0.15$. This shows there is a rhombohedral distortion due to sodium doping.

Table 1. Crystallographic data of $La_{0.7}Ca_{0.3-y}Na_yMnO_3$ for various (Na) concentrations (y).

y	a (Å)	b (Å)	c (Å)	α (deg)	Space group	Structure
0.0	5.47	7.736	5.497	—	*Pbmn*	Orthorhombic
0.05	5.472	—	—	60.005	$R\bar{3}c$	Rhombohedral
0.10	5.457	—	—	60.31	$R\bar{3}c$	Rhombohedral
0.15	5.452	—	—	60.37	$R\bar{3}c$	Rhombohedral

i.e. the area (say)

$$\delta = \int_0^{t_m} V_i(t)\,\mathrm{d}t$$

is calculated by using the final (averaged) data. In calculating the effective cross-sectional area of the pick-up coils mean diameters are considered.

3. Results

3.1. Structural studies with x-ray diffraction

XRD data of the samples at room temperature were recorded with a Philips PW1710 diffractometer using Cu Kα radiation with Ni filter. The XRD pattern of two samples, one without Na ($y = 0.0$) and the other with maximum Na substitution ($y = 0.15$), are shown in figures 3(a) and (b), respectively. It is clear from the diffraction pattern that the synthesized samples are single phase with no measurable impurity phases. Structural analysis of the samples was performed using the program DBWS. The refined values of the structural parameters are given in table 1. It was observed that the undoped $La_{0.7}Ca_{0.3}MnO_3$ sample shows an orthorhombic perovskite structure. Space group *Pbmn* was used in the refinement for the undoped sample whereas the $R\bar{3}c$ space group in the hexagonal axes was used for all the Na doped samples. It is clear from the analysis that the Na doped samples produces rhombohedral distortion, which is consistent with the previously reported results [16, 19]. The transition from the orthorhombic

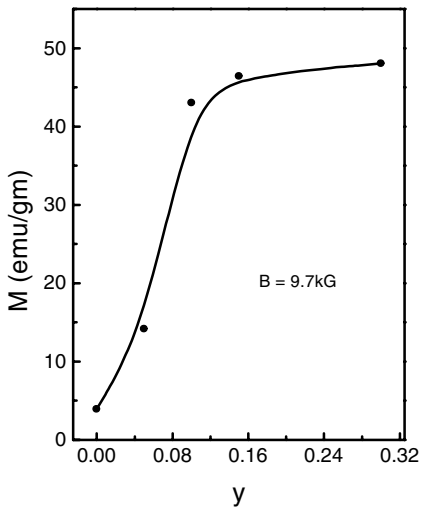

Figure 4. Magnetization (M) versus doping concentration (y) plot at room temperature with $B = 9.7$ kG.

phase to the rhombohedral phase due to Na doping indicates that structural disorder decreases and hence the Mn–O–Mn bond angle increases. The distortion in the MnO_6 octahedron becomes less, with the Mn–O–Mn bond angle moving towards 180°. Less distortion in the crystal structure reduces the possibility of charge localization and hence samples become more conducting, which is further supported by resistivity data. In this regard it should be mentioned that Roy *et al* [19] have shown that, for the $La_{1-x}Na_xMnO_3$ systems, increased Na doping drives the structure to become more cubic, resulting an increase in one-electron bandwidth. Consequently the possibility of greater overlapping is increased and hence greater conductivity is observed.

3.2. Magnetic properties

A vibrating sample magnetometer with three different magnetic fields of values 8.306, 9.036 and 9.67 kG performed magnetization measurements at 300 K and a lab-made susceptometer with external magnetic field $H = 0$ and frequency 1024 Hz was used to measure the low temperature (down to 77 K) susceptibility data. The magnetization (M) versus sodium concentration (y) plot (figure 4) clearly indicates that, at room temperature, the magnetization increases with increasing y. The paramagnetic phase thus approaches the ferromagnetic phase with increasing Na doping. This can be explained by considering that with increasing doping concentration (y) the ratio of Mn^{4+}/Mn^{3+} increases (discussed later) which favours the ferromagnetic DE interaction. We also see from the data that magnetization almost saturates after $y \geqslant 0.1$ and does not increase much with further increases in y. An almost similar result is explained by Roy *et al* [19] as the completion of the rhombohedral phase for $y \geqslant 0.1$ that contributes to the magnetization. We believe that, in addition to the above argument, in the high doping regime the increase in Mn^{4+} ions favours a super-exchange interaction (Mn^{4+}–O–Mn^{4+}) over the DE interaction and hence the magnetization almost saturates. The T_C values of all the samples are listed in table 2. Approximately the same value of T_p and T_C indicate that the samples are of good quality with a negligible grain boundary effect [21].

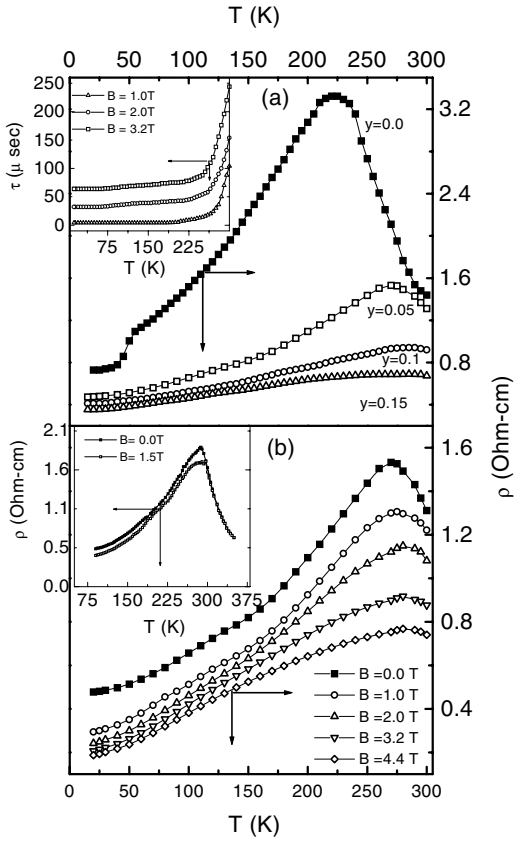

Figure 5. (a) Resistivity versus temperature plot at zero magnetic field for different Na concentrations. Inset shows the nature of thermal variation of the relaxation time (ι) for a typical sample with $y = 0.05$ in a magnetic field. (b) Resistivity versus temperature plot for $La_{0.7}Ca_{0.25}Na_{0.05}MnO_3$ with different strengths of the pulsed magnetic field. Inset shows the resistivity versus temperature plot for the same sample with $B = 0.0$ and 1.5 T constant field.

Table 2. Some important data of all the prepared Na doped $La_{0.7}Ca_{0.3-y}Na_yMnO_3$ samples obtained from magnetization and resistivity measurements (both in the presence and in the absence of the pulsed magnetic field B indicated).

			ρ (Ω cm)		T_p (K)			% MR ($B = 4.4$ T)		
y	Mn^{4+}/Mn^{3+}	M (emu g^{-1}) ($B = 9.7$ kG)	$T = 300$ K	$T = T_p$	$B = 0$ T	$B = 2.0$ T	$B = 4.4$ T	$T = T_p$	$T = 300$ K	T_C (K) $B = 0$ T
0.0	0.428	3.9491	1.44	3.24	220	230	235	61.27	30.59	220
0.05	0.538	14.162	1.31	1.53	270	276	280	50.86	44.88	270
0.10	0.666	43.036	0.91	0.94	283	288	291	65.82	64.55	276
0.15	0.818	46.422	0.67	0.68	287	292	295	77.09	77.09	289

3.3. Transport properties

For samples with different Na concentrations ($y = 0.0, 0.05, 0.1, 0.15$), the resistivity in the low temperature region (below T_p) presents a metal-like behaviour (i.e. $d\rho/dT > 0$) and, as the temperature is increased, a sharp transition from the metal to insulator phase is seen at

T_p, very close to the corresponding Curie temperature T_C [21] of the sample (figure 5(a)). The maximum resistivity ρ_{max} (peak value) decreases and T_p shifts to higher temperature as y increases (table 2). This increase in conductivity with Na doping is considered to be associated with the increase of the ratio of Mn^{4+}/Mn^{3+}, which in turn contributes to the enhancement of charge carriers (holes in the present case) in the e_g band. This is in accordance with the suggestions made by others [19]. The values of Mn^{4+}/Mn^{3+} with increasing y, obtained from the valency calculations (table 2), supports this argument. The cation valency distribution can be represented as $La^{3+}_{1-x}Ca^{2+}_{x-y}Na_y(Mn^{3+}_{1-(x+y)}Mn^{4+}_{x+y})O_3$. Hence, for every y amount of increase in Na ions, there will be an $(x + y)$ amount of increase in Mn^{4+} ions and, as a consequence, for a small amount of Na doping there will be a large number of charge carriers (compared to Ca doping for instance) and thus resistivity is decreased.

The temperature dependence of resistivity measured both in the presence and in the absence of a pulsed magnetic field (maximum 4.4 T) on a typical sample, namely $La_{0.7}Ca_{0.25}Na_{0.05}MnO_3$, is shown in figure 5(b). Similar behaviour is also obtained for other samples of this group (table 2). Application of a pulsed magnetic field causes a significant decrease in the resistivity, shifting the resistivity peak to the high temperature region. During the field pulse, the spins favourably orient themselves and consequently the charge carriers suffer less scattering, showing a decrease in resistivity. To compare the pulsed field magnetoresistance data with the corresponding constant field result, we have shown in the inset of figure 5(b) the variation of resistivity with temperature of the same sample for zero and 1.5 T DC fields. Interestingly, we found that the thermal variation of resistivity measured under a constant DC field (1.5 T) is similar to that measured under a pulsed field. We, however, noticed some interesting temperature-dependent relaxation time behaviour, i.e. the time taken by the sample to return to the normal state (zero field state) after the pulsed field is switched off. The plot of this relaxation time (ι) as a function of temperature for a typical sample (with $y = 0.05$) is shown in the inset of figure 5(a). It is seen that the relaxation time (ι), depending on the magnetic field strength, is related to the magnetic spin ordering and falls sharply around T_C and remains almost constant in the low temperature FM phase (figure 5(a) inset). Similar results are also found for the other samples. A nearly constant value of ι in the ferromagnetic region indicates the most ordered state behaviour. It is also noticed that the nature of the (ι–T) curve depends on sample grain size. So ι is also related to the grain size of the samples, indicating the importance of the pulsed field study. In this regard it can be mentioned that, with the application of magnetic field or lowering the temperature below MIT, the FM clusters embedded in the paramagnetic matrix form a connecting path and hence percolation occurs. In the present system, due to momentary excitation (pulsed field), some spins in the paramagnetic matrix becomes polarized to increase the number of FM clusters, hence enhancing the conductivity. After the withdrawal of the field, these momentarily formed FM clusters will return to their normal (unpolarized) state with an observed relaxation time (ι). Due to decreasing grain size, the size of the FM clusters would decrease and hence the connectivity between the FM clusters at low temperature would suffer. Therefore an increase of ρ and ι is expected in this case. Hence, by measuring the relaxation time, the mixed phase tendency of these manganites can be well studied. We believe this is a more important physical issue for our future investigation that pulsed field measurements could probe.

A plot of T_p versus alkali metal ion concentration (y) shows an almost exponential rise of T_p with increasing sodium content (figure 6(a)). With increasing y, ρ_{max} first decreases sharply and then gradually approaches a minimum value (inset of figure 6(a)). This observation can be explained by the fact that, in the low doping regime ($y \leqslant 0.1$), the Mn^{4+}/Mn^{3+} ratio is favourable to ferromagnetism and hence the FM-metallic state is extended with increasing y. With a further increase in doping level, the Mn^{4+} concentration increases and the

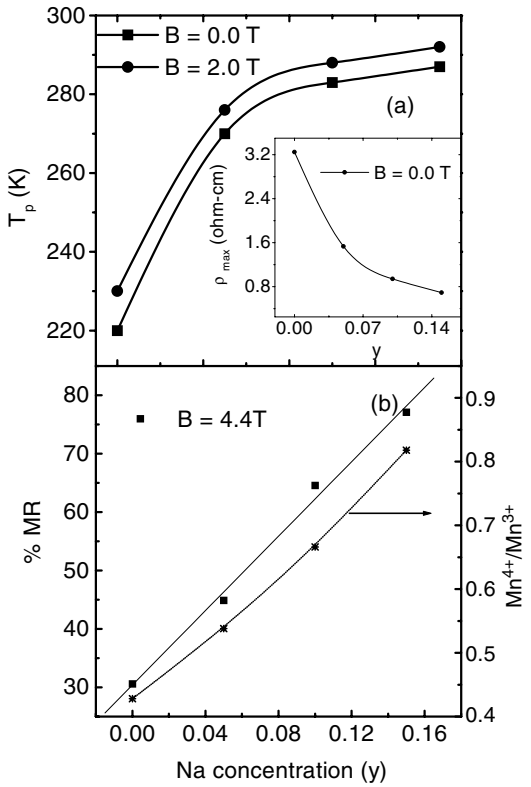

Figure 6. (a) Transition temperature T_p versus Na concentration y plot for $B = 0$ and 2.0 T. Inset shows the variation of maximum resistivity ρ_{max} with y for $B = 0$ T. (b) % MR versus y plot for different samples with $B = 4.4$ T at 295 K (full curve) and Mn^{4+}/Mn^{3+} ratio as a function of y (dotted curve).

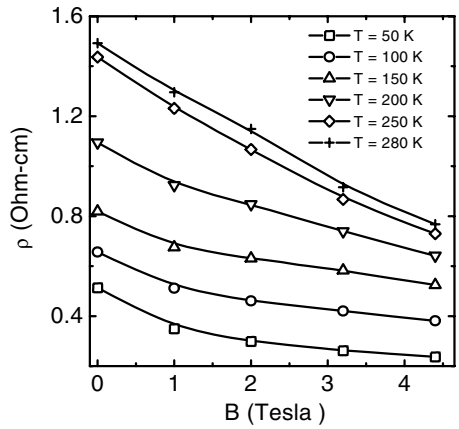

Figure 7. ρ versus magnetic field plot for $La_{0.7}Ca_{0.25}Na_{0.05}MnO_3$ at different temperatures.

superexchange interaction (Mn^{4+}–O–Mn^{4+}) becomes predominant over the hopping interaction and conclusively the increase of T_p and decrease of ρ_{max} with increasing y becomes much

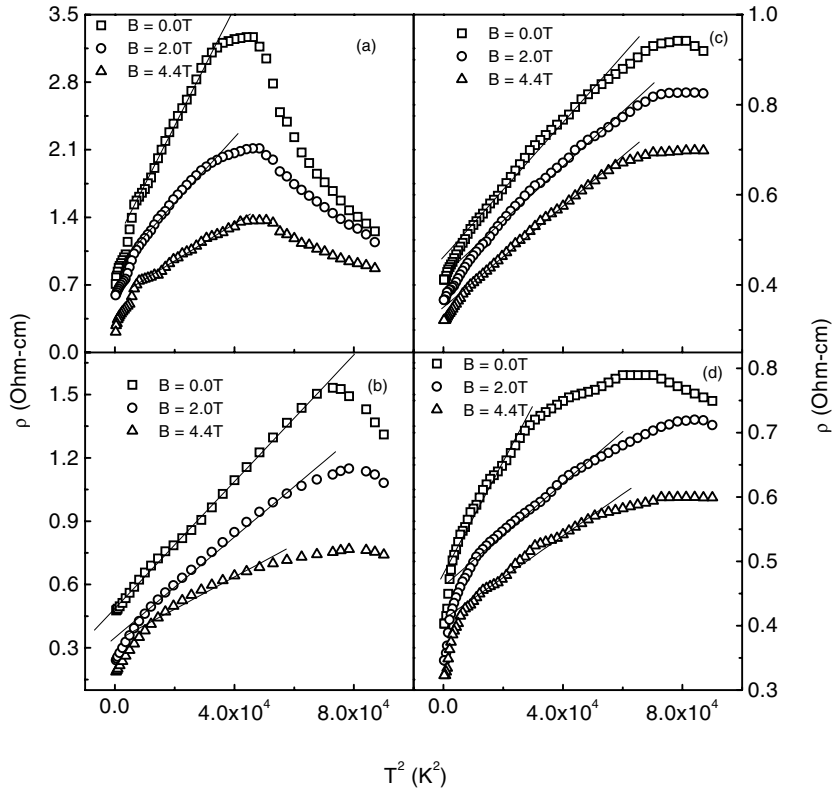

Figure 8. Linear fit of the low temperature (FM region) resistivity data with a T^2 term (equation (1)) for the sample: (a) $y = 0.0$, (b) $y = 0.05$, (c) $y = 0.1$, (d) $y = 0.15$.

smaller. From figure 6(b) one finds that % MR at room temperature with the maximum available field $B = 4.4$ T increases almost linearly with increasing sodium content. The field dependence of resistivity ρ of a sample $La_{0.7}Ca_{0.25}Na_{0.05}MnO_3$ as a function of applied field at different temperatures plotted in figure 7 shows that, below T_p, the field dependence of ρ is much smaller, indicating the ordering of magnetic spins in the FM state. This behaviour is also reflected from the thermal variation of ι below T_p as discussed above. At 300 K, a maximum magnetoresistance ratio $(\Delta\rho/\rho_0) \times 100[\Delta\rho = \rho_0(H = 0) - \rho(H)]/[\rho(H = 0)]$ is found to be as high as 77% for the sample with $y = 0.15$ under a pulsed magnetic field of 4.4 T.

In the low temperature ferromagnetic-metallic phase, the temperature dependence of the resistivity for all the samples both in the presence and in the absence of the pulsed magnetic field can be well fitted (figure 8) by an equation of the form

$$\rho(T) = \rho_0 + \rho_2 T^2 \tag{1}$$

where the temperature-independent part ρ_0 is the resistivity due to domain, grain boundary and other temperature-independent scattering mechanisms [22, 23]. Some authors have explained the $\rho_2 T^2$ by the electron–electron scattering process [23] but, following Mott [24], the ρ–T^2 behaviour in a ferromagnet is due to magnon scattering. We also believe that the spin scattering cannot be neglected in the low T regime, as the measured data can be best explained by electron–spin scattering. The best fit parameters obtained from fitting the low temperature metallic part of the resistivity data with equation (1) are shown in table 3. As expected, the temperature-

Table 3. The values of the parameters ρ_0 and ρ_2 of all the $La_{0.7}Ca_{0.3-y}Na_yMnO_3$ samples obtained from fitting the low temperature ($T < T_p$) resistivity data with equation (1) (both in the presence and in the absence of a magnetic field B).

	ρ_0 (Ω cm)			ρ_2 (Ω cm K^{-2})		
y	$B = 0.0$ T	$B = 2.0$ T	$B = 4.4$ T	$B = 0.0$ T	$B = 2.0$ T	$B = 4.4$ T
0.0	1.13	0.866	0.566	6.09×10^{-5}	3.40×10^{-5}	1.92×10^{-5}
0.05	0.483	0.349	0.236	1.52×10^{-5}	1.28×10^{-5}	1.27×10^{-5}
0.10	0.463	0.421	0.355	7.24×10^{-6}	6.06×10^{-6}	5.43×10^{-6}
0.15	0.451	0.447	0.397	6.07×10^{-6}	4.53×10^{-6}	3.77×10^{-6}

Table 4. Some important high temperature estimated data from all the prepared Na doped $La_{0.7}Ca_{0.3-y}Na_yMnO_3$ samples obtained both in the presence and in the absence of a pulsed magnetic field.

	W_H (meV)		$N(E_F)$ (eV^{-1} cm^{-3})		
y	0.0 T	1.5 T	$B = 0.0$ T	1.5 T	$\gamma = 2W_H/h\nu_{ph}$
0.0	103.17	82.57	3.8×10^{20}	17.9×10^{20}	4.69
0.05	91.84	72.53	6.94×10^{20}	7.15×10^{20}	3.74
0.10	85.52	68.29	8.52×10^{20}	8.78×10^{20}	3.16
0.15	80.31	67.56	10.06×10^{20}	10.96×10^{20}	2.85

independent term (ρ_0) for all the polycrystalline samples decreases significantly with magnetic field but the influence of the magnetic field on the ρ_2 term is comparatively small. It is likely that the mechanism responsible for MR in the system is the influence of the magnetic field on the ordering of magnetic domains. As the pulsed magnetic field strength increases, the size of the domain boundary decreases and ρ_0 becomes smaller [25]. The decrease of ρ_2 in a magnetic field is due to the suppression of spin fluctuation in the applied magnetic field (proportional to $B^{-1/3}$) [22]. In this regard it should be mentioned that the range of validity of the T^2 dependence decreases due to application of an appreciable high field. As the magnetic field polarizes the randomly oriented spins the scattering effect is diminished and so the temperature region over which the scattering mechanism dominates decreases.

All the resistivity data, above the transition temperature T_p, have earlier [26, 27] been fitted with variable range hopping (VRH) of charge carriers. Recently Viret *et al* and Pal *et al* have applied a VRH conduction mechanism in systems like La–Ca–Mn–O, La–Mn–O, La–Pb–Mn–O, etc, at higher temperatures above T_p. Similarly our data between T_p and 320 K also fit the VRH model quite well. This model in three-dimensional cases can be written as

$$\sigma_{dc} = \sigma_0 \exp[-(T_0/T)]^{1/4} \tag{2}$$

where T_0 is a constant [$=18\alpha^3/k_B N(E_F)$], α is the electron wavefunction decay constant, k_B is Boltzmann's constant and $N(E_F)$ is the density of states at the Fermi level, which can be calculated from the slope of the plot of log σ_{dc} versus $T^{-1/4}$ curves (shown in figures 9(a) and (b)). The best fit occurs with $T_0 \sim 10^6$ for both La–Ca–Mn–O and La–Ca–Na–Mn–O, which is in good agreement with the previously reported results [27]. We have also calculated T_0 for different samples in the presence of magnetic fields. T_0 is found to decrease with increasing magnetic field strength. From equation (2) we also estimated $N(E_F)$ (table 4) using $\alpha = 2.22$ nm^{-1} as used by Pal *et al*. The values of $N(E_F)$ are comparable to those obtained by Coey *et al* [26] ($N(E_F) \sim 4 \times 10^{22}$ eV cm^{-3} for the La–Ca–Mn–O system) and Pal *et al* [27] ($N(E_F) \sim 5.99 \times 10^{22}$ eV cm^{-3} for the La–Pb–Mn–O system). The $N(E_F)$

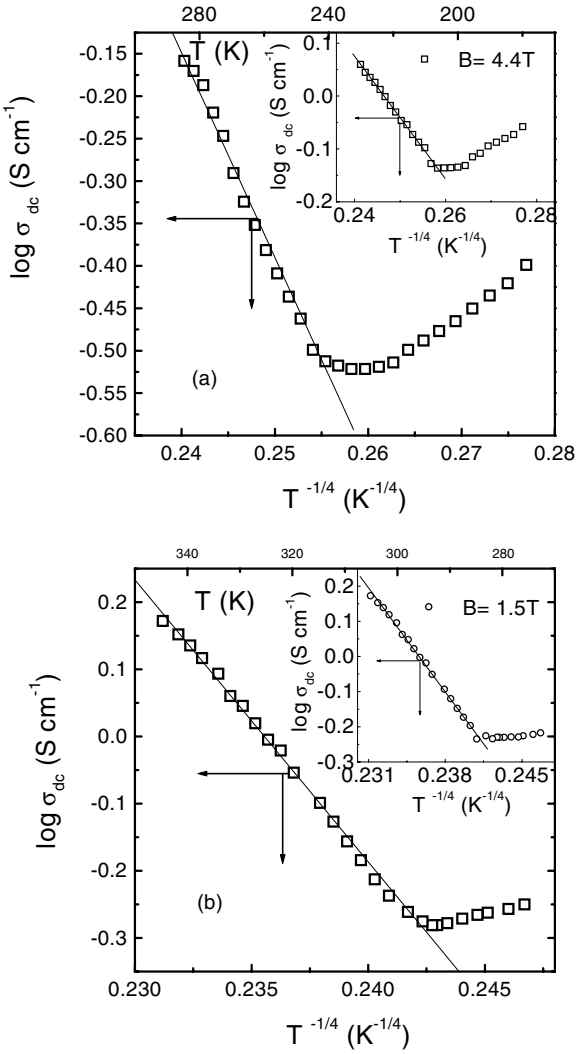

Figure 9. Variation of conductivity $\log \sigma_{dc}$ as a function of $T^{-1/4}$ (equation (2)) for (a) $La_{0.7}Ca_{0.3}MnO_3$ with $B = 0.0$ T. Inset shows the plot with $B = 4.4$ T. (b) $La_{0.7}Ca_{0.25}Na_{0.05}MnO_3$ with $B = 0.0$ T. Inset shows the plot with $B = 1.5$ T. Full lines are the best fit to the VRH model.

value for the present sample is found to be increasing with the application of magnetic field. $N(E_F)$ is found to be $\sim 4.46 \times 10^{21}$ eV cm^{-3} (with $B = 4.4$ T) for the undoped La–Ca–Mn–O and $\sim 7.153 \times 10^{20}$ eV cm^{-3} (with $B = 1.5$ T) for the Na (5%) doped La–Ca–Na–Mn–O sample (all the other values are listed in table 4). It is noticed that, for the Na doped sample, $N(E_F)$ is much higher than that of the undoped sample, indicating an appreciable increase in the number of charge carriers and consequently showing an increase in the conductivity of the Na doped sample. Also the application of magnetic field decreases the localization length which in turn increases the number of delocalized charge carriers causing increased $N(E_F)$.

It should be mentioned here that the VRH model could not be extended to fit well the data above 320 K (between 320 and 350 K). Recently it has been shown by Banerjee *et al*

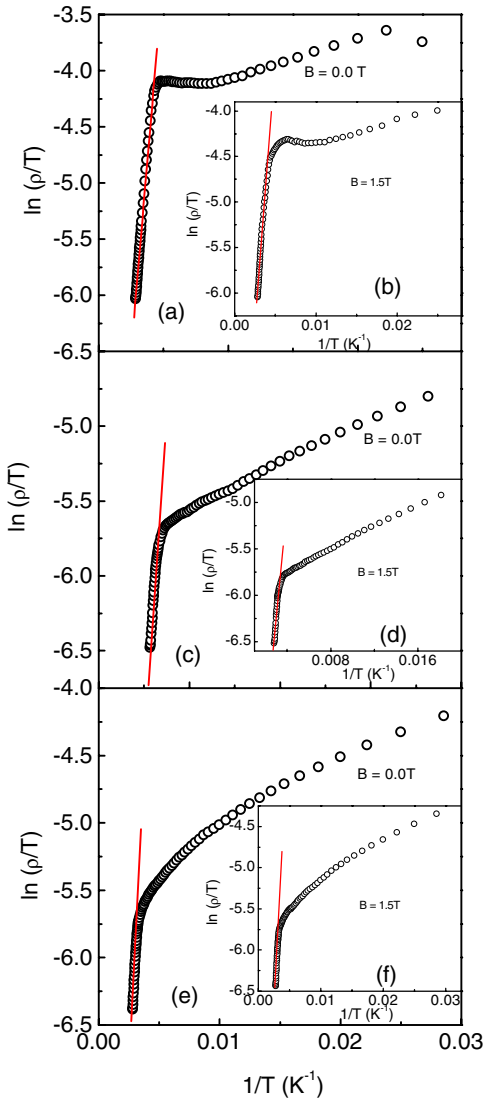

Figure 10. Variation of $\ln(\rho/T)$ as a function of inverse temperature $1/T$ with $y = 0.0$ for (a) and (b); $y = 0.10$ for (c) and (d); $y = 0.15$ for (e) and (f). Inset graphs (b), (d) and (f) shows the plot with pulsed field $B = 1.5$ T. Full lines are the best fit to the SPH model.

(This figure is in colour only in the electronic version)

[27, 28] that the conductivity data between T_p and $\theta_D/2$ can only be well fitted with the VRH model, while high temperature ($T > \theta_D/2$, θ_D being the Debye temperature) resistivity data of the Cr doped and undoped La–Pb–Mn–O manganite samples can be well fitted with the thermally activated small polaron hopping (SPH) model. Similar behaviour is also exhibited by the present Na doped system. For the samples with higher T_p values (like the present samples), the VRH region is small. So it is rather difficult to judge which of the two models is most appropriate. It is, however, noticed that the high temperature ($T > \theta_D/2$) conductivity data between 320 and 350 K for the Na doped samples (figure 10) better fit the SPH model

of Mott, namely $\rho/T = \rho_\alpha \exp(E_p/k_BT)$, where $\rho_\alpha = [k_B/\nu_{ph}\mathrm{Ne}^2R^2C(1-C)]\exp(2\alpha R)$, where N is the number of ion sites per unit volume (obtained from the density data), R is the average intersite spacing obtained from the relation $R = (1/N)^{1/3}$, E_p is the activation energy for hopping conduction estimated from the conductivity data, C is the fraction of sites occupied by a polaron, α is the electron wavefunction decay constant obtained from fitting the experimental conductivity data and ν_{ph} is the optical phonon frequency (estimated from the relation $h\nu_{ph} = k_B\theta_D$). Following the procedure of our earlier work [27] an estimation of the electron–phonon (e–ph) coupling constant (γ) of the sample is made from the relation $\gamma = 2W_H/h\nu_{ph}$ [29], when polaron hopping energy W_H is estimated from the relation $W_H = E_p - E_S$, where E_S is the activation energy obtained from the thermoelectric power [30]. Millis *et al* [4] have shown that γ is a crucial parameter controlling T_C which is close to the MIT temperature T_p for the present system. For the present system under investigation the estimated values of γ vary from 4.69 to 2.85 for $y = 0.0$–0.15 as shown in table 4. Hence there is a decrease in the e–ph coupling constant with an increase of y and thereby an increase of T_p is obtained, in agreement with the theory proposed by Millis *et al*. For the La–Na–Mn–O system showing an increase of T_p with Na doping, Rao *et al* [17] predicted that Na doping induces a transition from strong Hund coupling between e_g and t_{2g} spins to weak Hund coupling. In addition they argued that MIT corresponds to a transition from a strong e–ph coupling, giving rise to a high resistivity, to a weak e–ph coupling that favours low resistivity. From the calculation of the e–ph coupling constant γ we have confirmed that an increase of T_p with Na doping is associated with a decrease of γ. In fact, addition of Na leads the system from the polaronic hopping conduction regime to the electronic conduction regime. It has been shown theoretically by Mott and Austin [31] that a larger value of $\gamma > 4$ is required for the polaron formation in purely semiconducting samples. From the estimated values of γ we find that only for $y = 0.0$, i.e. the $La_{0.7}Ca_{0.3}MnO_3$ sample, the value of $\gamma > 4$. With increasing y, the electron–phonon interaction decreases and $\gamma < 4$ for samples with $y = 0.05$–0.15, which signifies that, in the Na doped systems, the polaron formation decreases and hence as y increases electronic conduction plays a major role. The conductivity data also shows that, with increasing y, conductivity increases, which further specifies a decreasing e–ph interaction. This is considered to be one of the most important effects of Na doping on manganite samples. Interestingly, our present investigation (unpublished) with Li in the same system shows large changes of both T_p and transport behaviour.

4. Conclusions

Finally, in conclusion, magnetotransport properties of $La_{1-x}Ca_{x-y}Na_yMnO_3$ for $x = 0.3$ and $0 \leqslant y \leqslant 0.15$ are measured, for the first time to the best of our knowledge, under a pulsed magnetic field (0.0–4.4 T), showing identical transport behaviour to that observed under a DC magnetic field. A maximum of 77% magnetoresistance has been observed at 300 K for the $La_{0.7}Ca_{0.15}Na_{0.15}MnO_3$ ceramic sample with a pulsed magnetic field of $B = 4.4$ T. Monovalent alkali-metal-like Na doping in a La–Ca–Mn–O system drives the system towards higher conductivity and a higher metal–insulator transition temperature regime, leading to a CMR effect around room temperature. Furthermore, an increase of conductivity in the La–Ca–Mn–O system with increasing Ca is different from the corresponding increase of T_p in the present Na doped system (partially replacing Ca and keeping La fixed). Since T_p can be varied around room temperature only by small increases of Na at the Ca site, the present Na doped system might be a potential candidate for device applications. We would also like to add that the pulsed field technique, used in the present measurements, is a convenient technique, which would be very useful for quick and accurate measurement of magnetotransport properties of

rare earth manganites, superconducting and other related materials of current interest. The temperature, magnetic field and sample grain-size-dependent relaxation time (ι) observed in a pulsed field may also be used to determine the field-dependent spin ordering in the low temperature ferromagnetic phase as well as the grain size effect on the transport and magnetic properties in the mixed phase separation picture. This might be an important use of the pulsed field technique. Finally we would like to mention that the magnetotransport behaviour of the K-doped $La_{1-x}Ca_{x-y}K_yMnO_3$ system (not reported in this paper) is also found to be similar to that of the Na-doped system, while it is quite different from that of the corresponding Li doped system, which will be discussed elsewhere.

Acknowledgments

The authors are grateful to the Department of Science and Technology, Government of India for financial support. We are also grateful to Professor E Rozenberg and Dr D Mogilyansky for their kind help during the magnetization measurements. One of the authors (BKC) is also grateful to Professor H D Yang, Physics Department, National Sun Yat Sen University, Taiwan for his comments and interest in this work. The author BKC is also grateful to NSC, Taiwan (ROC) for partial financial assistance during his stay at the Department of Physics, NSYS University.

References

[1] Van Santen J H and Jonker G H 1950 *Physica* **7** 599
[2] Jin S, Tiefel T H, McCormack M, Fastnacht R A, Ramesh R and Chen L H 1994 *Science* **264** 413
[3] Zener C 1951 *Phys. Rev.* **82** 403
[4] Millis A J, Littlewood P B and Shraiman B I 1995 *Phys. Rev. Lett.* **74** 5144
[5] Jirak Z, Damay F, Hervieu M, Martin C, Raveau B, André G and Bourée F 2000 *Phys. Rev.* B **61** 1181
[6] Hwang H Y, Cheong S-W, Radaelli P G, Marezio M and Batlogg B 1995 *Phys. Rev. Lett.* **75** 914
[7] Abdelmoula N, Dhahri E, Guidara K and Joubert J C 1999 *Phase Transit.* **69** 215
[8] Sun J R, Rao G H, Gao X R, Liang J K, Wong H K and Shen B G 1999 *J. Appl. Phys.* **85** 3619
[9] Fan X J, Zhang J H, Li X G, Wu W B, Wan J Y, Lee T J and Ku H C 1999 *J. Phys.: Condens. Matter* **11** 3141
[10] Rodriguez-Martinez L M and Attfield J P 1996 *Phys. Rev.* B **54** R15622
[11] Topfer J and Goodenough J B 1997 *J. Solid State Chem.* **130** 117
[12] Gonzalez-Calbet J M *et al* 1999 *J. Solid State Chem.* **148** 158
[13] Abdelmoula N, Guidara K, Cheikhrouhou A, Dhahri E and Joubert J C 2000 *J. Solid State Chem.* **151** 139
[14] Archibald W, Zhou J-S and Goodenough J B 1996 *Phys. Rev.* B **53** 14445
[15] van Roosmalen J A M, van Vlaanderen P and Cordfunke E H P 1995 *J. Solid State Chem.* **114** 516
[16] Boudaya C, Laroussi L, Dhahri E, Joubert J C and Cheikhrouhou A 1998 *J. Phys.: Condens. Matter* **10** 7485
[17] Rao G H, Sun J R, Bärner K and Hamad N 1999 *J. Phys.: Condens. Matter* **11** 1523
[18] Abdelmoula N, Cheikhrouhou A and Reversat L 2001 *J. Phys.: Condens. Matter* **13** 449
[19] Roy S, Guo Y Q, Venkatesh S and Ali N 2001 *J. Phys.: Condens. Matter* **13** 9547
[20] Coey J M D, Viret M and Ranno L 1995 *Phys. Rev. Lett.* **75** 3910
[21] Mahendiran R, Mahesh R, Raychaudhuri A K and Rao C N R 1995 *J. Phys. D: Appl. Phys.* **28** 1743
[22] Jeffrey Synder G, Hiskes R, Dicarolis S, Beasley M R and Geballe T H 1996 *Phys. Rev.* B **54** R15606
[23] Urushibara A *et al* 1995 *Phys. Rev.* B **51** 14103
[24] Mott N F 1974 *Metal–Insulator Transitions* (London: Taylor and Francis)
[25] Schiffer P, Ramirez A P, Bao W and Cheong S W 1995 *Phys. Rev. Lett.* **75** 3336
[26] Viret M, Ranno L and Coey J M D 1997 *Phys. Rev.* B **55** 8067
[27] Pal S, Banerjee A, Rozenberg E and Chaudhuri B K 2001 *J. Appl. Phys.* **89** 4955
[28] Aritra B, Pal S, Rozenberg E and Chaudhuri B K 2001 *J. Phys.: Condens. Matter* **13** 9489
[29] Mott N F and Davis E A 1971 *Electronics Process in Non Crystalline Materials* (Oxford: Clarendon)
[30] Aritra B, Pal S, Bhattacharya S, Yang H D and Chaudhuri B K 2001 *Phys. Rev.* B **64** 104428 and references therein
[31] Mott N F and Austin I G 1969 *Adv. Phys.* **18** 41